PHYSICAL REVIEW B VOLUME 9, NUMBER 2 15 JANUARY 1974

Transient photovoltaic effects in anisotropic semiconductors*

A. Subramanian, S. J. Gordon, and J. F. Schetzina
Department of Physics, North Carolina State University, Raleigh, North Carolina 27607
(Received 3 August 1973)

A time-dependent ambipolar theory describing transient photovoltaic effects that occur in illuminated anisotropic semiconductors is discussed. The formalism is such that the theory may be used to describe transients in the transverse Dember, photopiezoresistance, and photomagnetoelectric effects. An anisotropic semiconductor having one surface uniformly illuminated with light of time-varying intensity is considered and general expressions for the short-circuit current and open-circuit photovoltage per unit length are obtained. Particular solutions for several different illuminations are included. Experiments undertaken to observe the transient photopiezoresistance effect in germanium, in which photovoltages as large as 1 V were recorded, are also described. A comparison between theory and experiment is included.

I. INTRODUCTION

When the surface of an anisotropic semiconductor is exposed to light that is strongly absorbed, a carrier-concentration gradient forms normal to the surface and this is accompanied by the diffusion of excess carriers into the bulk. As a consequence of anisotropy, however, the diffusion of electrons generally proceeds in a direction different from that of holes. Because of this, a photovoltage develops continuously along the length of the specimen. In addition, if the ends of the specimen are shorted, an electrical current flows. The photovoltaic effect occurs in naturally anisotropic semiconductors as the *transverse Dember effect.*[1,2] Similar effects are also observable in cubic semiconductors for which anisotropies have been externally created. In the *photopiezoresistance effect*[3-6] elastic strain produces the requisite transport anisotropies, whereas in the well-known *photomagnetoelectric effect*[7,8] an external magnetic field is employed for this purpose. All of these effects arise from a common cause, the preferential drift and diffusion of photogenerated electrons and holes, and they can all be treated with a single phenomenological theory. In this paper a time-dependent ambipolar theory is discussed, one that may be employed to describe transients in all of the above effects.

In Sec. II, an anisotropic semiconductor having one surface uniformly illuminated with an arbitrary (time-dependent) light flux is considered. The equations needed to describe the photovoltaic effect are first presented. The intrinsic case, for which the effect is largest, is then discussed in detail and general expressions for the short-circuit current I_{sc} and open-circuit photovoltage per unit length V_{oc} are obtained. Particular solutions for several types of transient illuminations are included. The extension of the theory to include the extrinsic case is also discussed. In Sec. III, experiments designed to observe the transient photopiezoresistance effect in germanium are described and the experimental results are compared with the predictions of the ambipolar theory.

II. THEORY

Let us consider an anisotropic semiconductor having dimensions x_0, y_0, z_0 that is oriented as shown in Fig. 1. We assume the semiconductor to be characterized by electron and hole mobility tensors $\overleftrightarrow{\mu_n}$ and $\overleftrightarrow{\mu_p}$, that are anisotropic in the xy plane and whose principal axes *do not* coincide with the x and y axes of the specimen. Beginning at time $t=0$ the lower semiconductor surface at $y=0$ is uniformly illuminated with light of intensity $I_0(t)$. The time dependence of the illumination intensity is arbitrary. The following assumptions are made.

(a) The quasineutrality approximation holds such that the concentration of excess electrons δn is equal to the concentration of excess holes δp.

(b) The production of electron-hole pairs due to illumination occurs with quantum efficiency β and takes place *at the illuminated surface* and not in the bulk.

(c) $\vec{\nabla}\times\vec{E}=0$, where $\vec{E}$ is the local electric field. That is, we shall neglect effects due to time-dependent magnetic fields.

(d) End effects and trapping effects are negligible.

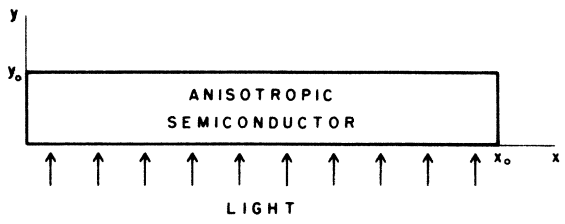

FIG. 1. Geometry of specimen considered in text. The z axis is out of the plane of the paper.

For the case to be considered, the electron and hole mobility tensors, $\overleftrightarrow{\mu}_n$ and $\overleftrightarrow{\mu}_p$, may be expressed in matrix form in the specimen coordinate system as[9]

$$\overleftrightarrow{\mu}_n = \begin{bmatrix} \mu_{nxx} & \mu_{nxy} & 0 \\ \mu_{nyx} & \mu_{nyy} & 0 \\ 0 & 0 & \mu_{nzz} \end{bmatrix}, \tag{1}$$

$$\overleftrightarrow{\mu}_p = \begin{bmatrix} \mu_{pxx} & \mu_{pxy} & 0 \\ \mu_{pyx} & \mu_{pyy} & 0 \\ 0 & 0 & \mu_{pzz} \end{bmatrix}. \tag{2}$$

For nondegenerate semiconductors, the corresponding diffusivities are given by

$$\overleftrightarrow{D}_n = (kT/e)\overleftrightarrow{\mu}_n , \tag{3}$$

$$\overleftrightarrow{D}_p = (kT/e)\overleftrightarrow{\mu}_p . \tag{4}$$

Likewise, the conductivity tensors $\overleftrightarrow{\sigma}_n$, $\overleftrightarrow{\sigma}_p$, and $\overleftrightarrow{\sigma}$ are defined by

$$\overleftrightarrow{\sigma}_n = ne\overleftrightarrow{\mu}_n , \tag{5}$$

$$\overleftrightarrow{\sigma}_p = pe\overleftrightarrow{\mu}_p , \tag{6}$$

$$\overleftrightarrow{\sigma} = \overleftrightarrow{\sigma}_n + \overleftrightarrow{\sigma}_p , \tag{7}$$

where n and p are electron and hole concentrations, respectively.

We seek expressions for the current I_{sc} that flows in the illuminated semiconductor when the ends along x are short circuited and for the photovoltage per unit length V_{oc} that develops under open-circuit conditions. Using the methods discussed by Shah and Schetzina,[5] an excess-carrier continuity equation for the case under consideration may be obtained in the form

$$\frac{\partial}{\partial y}\left(D^*\frac{\partial \delta p}{\partial y}\right) - v^*\frac{\partial \delta p}{\partial y} - \frac{\delta p}{\tau} = \frac{\partial \delta p}{\partial t} . \tag{8}$$

Likewise, expressions for J_x, the x component of the total current density, and J_{py}, the y component of the hole current density, are obtained as

$$J_x = -eaD^*\frac{\partial \delta p}{\partial y} + \sigma^* E_x , \tag{9}$$

$$J_{py} = -eD^*\frac{\partial \delta p}{\partial y} + p^* ev^* . \tag{10}$$

In the above expressions τ is the excess-carrier lifetime and

$$D^* = \frac{(n+p)D_{nyy}D_{pyy}}{nD_{nyy} + pD_{pyy}} , \tag{11}$$

$$a^* = \frac{\sigma_{pyx}}{\sigma_{pyy}} - \frac{\sigma_{nyx}}{\sigma_{nyy}} , \tag{12}$$

$$a = \frac{\sigma_{pxy}}{\sigma_{pyy}} - \frac{\sigma_{nxy}}{\sigma_{nyy}} , \tag{13}$$

$$p^* = \frac{pn\sigma_{yy}}{n\sigma_{nyy} + p\sigma_{pyy}} , \tag{14}$$

$$\sigma^* = \sigma_{xx} - \frac{\sigma_{xy}\sigma_{yx}}{\sigma_{yy}} , \tag{15}$$

$$v^* = a^*\left(\frac{\sigma^\dagger}{p^* e}\right)E_x , \tag{16}$$

where

$$\sigma^\dagger = \frac{\sigma_{nyy}\sigma_{pyy}}{\sigma_{nyy} + \sigma_{pyy}} . \tag{17}$$

The parameters a^* and a are dimensionless anisotropy factors. They are zero for an isotropic semiconductor.

If the semiconductor is intrinsic, considerable simplification occurs. Let us consider this case first. Upon changing to dimensionless variables $Y = y/L$ and $T = t/\tau$, where $L = (D\tau)^{1/2}$ is an effective diffusion length, Eqs. (8)–(10) may be written as

$$\frac{\partial^2 \delta p}{\partial Y^2} - R\frac{\partial \delta p}{\partial Y} - \delta p = \frac{\partial \delta p}{\partial T} , \tag{18}$$

$$J_x = -eav_d\frac{\partial \delta p}{\partial Y} + \sigma^* E_x , \tag{19}$$

$$J_{py} = -ev_d\frac{\partial \delta p}{\partial Y} + pev . \tag{20}$$

In the above equations

$$D = 2D_{nyy}D_{pyy}/(D_{nyy} + D_{pyy}) , \tag{21}$$

$$v = ea^*DE_x/2kT , \tag{22}$$

$$v_d = D/L , \tag{23}$$

$$R = v/v_d . \tag{24}$$

Under short-circuit conditions, $E_x = 0$; thus, using $I_{sc} = \int J_x\, dy\, dz$ and (19), one obtains

$$I_{sc} = z_0 eav_d L[\delta p(0, T) - \delta p(Y_0, T)] . \tag{25}$$

Under open-circuit conditions, $\int J_x\, dy\, dz = 0$. Using this fact and (19), one obtains $V_{oc} \equiv -E_{x(oc)}$ in the form

$$V_{oc} = \frac{av_d}{\mu^*}\left(\frac{\delta p(0, T) - \delta p(Y_0, T)}{p_0 Y_0 + \int_0^{Y_0}\delta p(Y, T)\,dY}\right). \tag{26}$$

In (26), p_0 is the equilibrium carrier concentration and $\mu^* = \sigma^*/pe$. We therefore seek a solution to (18) that satisfies the initial condition $\delta p(Y, 0) = 0$ and appropriate surface boundary conditions. Substitution of such a solution into (25) and (26) will then yield the desired results.

Under short-circuit conditions, the drift terms in (18) and (20) are zero since $E_x = 0$. We shall assume these terms to be negligible under open-circuit conditions as well. This will always be the

case in the small signal regime and also for moderately large signals provided the anisotropy factor a^* is small. With the above approximation, the continuity equation simplifies to

$$\frac{\partial^2 \delta p}{\partial Y^2} - \delta p = \frac{\partial \delta p}{\partial T} , \tag{27}$$

and the usual surface boundary conditions reduce to

$$\frac{\partial \delta p}{\partial Y} = S_1 \delta p - I \quad (\text{at } Y = 0) , \tag{28}$$

$$\frac{\partial \delta p}{\partial Y} = - S_2 \delta p \quad (\text{at } Y = Y_0) . \tag{29}$$

In (28) and (29), $I = \beta I_0 / v_d$, $S_1 = s_1 / v_d$, and $S_2 = s_2 / v_d$, where s_1 and s_2 are the surface recombination velocities at the illuminated and dark surfaces, respectively.

Equations (27)–(29) may be conveniently solved using Laplace transformation techniques. Upon making a Laplace transformation on T, one obtains the continuity equation

$$\frac{d^2 \delta \bar{p}}{dY^2} - \lambda^2 \delta \bar{p} = 0 , \tag{30}$$

where

$$\mathcal{L}(\delta p) = \delta \bar{p} = \int_0^\infty \delta p e^{-sT} dT \tag{31}$$

and $\lambda^2 = s + 1$. The boundary conditions transform as

$$\frac{d \delta \bar{p}}{dY} = S_1 \delta \bar{p} - \bar{I} \quad (\text{at } Y = 0) , \tag{32}$$

$$\frac{d \delta \bar{p}}{dY} = - S_2 \delta \bar{p} \quad (\text{at } Y = Y_0) , \tag{33}$$

where

$$\mathcal{L}(I) = \bar{I} = \int_0^\infty I e^{-sT} dT . \tag{34}$$

The transformed set of Eqs. (30)–(33) can be solved by standard means. The solution obtained may be written in the form

$$\delta \bar{p} = \bar{I} \bar{G} , \tag{35}$$

where

$$\bar{G} = \frac{S_0 \sinh \lambda(Y_0 - Y) + \lambda \cosh \lambda(Y_0 - Y)}{(\lambda^2 + S_1 S_2) \sinh \lambda Y_0 + (S_1 + S_2) \lambda \cosh \lambda Y_0} . \tag{36}$$

Inspection of (35) indicates that the excess-carrier concentration δp may be expressed as a convolution. Thus, we have

$$\delta p = \mathcal{L}^{-1}(\bar{I} \bar{G}) , \tag{37}$$

$$\delta p = \int_0^T I(T') G(T - T') dT' , \tag{38}$$

where, by the Laplace-Mellin inversion theorem,

$$G(Y, T) = \frac{1}{2\pi i} \int_{\epsilon - i\infty}^{\epsilon + i\infty} \bar{G} e^{sT} ds . \tag{39}$$

The above integral may be evaluated using the method of residues. When this is done one obtains

$$G(Y, T) = \sum_{n=1}^{\infty} C_n(Y) e^{-\nu_n T} . \tag{40}$$

In (40)

$$C_n(Y) = \frac{2\alpha_n [\alpha_n \cos \alpha_n (Y_0 - Y) + S_2 \sin \alpha_n (Y_0 - Y)]}{[(\alpha_n^2 - S_1 S_2) Y_0 - (S_1 + S_2)] \cos \alpha_n Y_0 + \alpha_n [(S_1 + S_2) Y_0 + 2] \sin \alpha_n Y_0} , \tag{41}$$

the α_n's are the positive roots of the transcendental equation

$$\cot \alpha Y_0 = \frac{\alpha^2 - S_1 S_2}{\alpha (S_1 + S_2)} , \tag{42}$$

and

$$\nu_n = \alpha_n^2 + 1. \tag{43}$$

Expressions for I_{sc} and V_{oc} may now be obtained by the substitution of Eqs. (38)–(41) into (25) and (26). This procedure gives, after integration and simplification,

$$I_{sc} = \gamma \sum_{n=1}^{\infty} A_n R_n(T) , \tag{44}$$

$$V_{oc} = \frac{a v_d}{\mu^*} \frac{\sum_{n=1}^{\infty} A_n R_n(T)}{p_0 v_d y_0 + \sum_{n=1}^{\infty} B_n R_n(T)} . \tag{45}$$

In the above equations $\gamma = z_0 e a L$ and

$$A_n = \frac{2\beta\alpha_n [\alpha_n (\cos \alpha_n Y_0 - 1) + S_2 \sin \alpha_n Y_0]}{[(\alpha_n^2 - S_1 S_2) Y_0 - (S_1 + S_2)] \cos \alpha_n Y_0 + \alpha_n [(S_1 + S_2) Y_0 + 2] \sin \alpha_n Y_0} , \tag{46}$$

$$B_n = \frac{2\beta [\alpha_n \sin \alpha_n Y_0 + S_2 (1 - \cos \alpha_n Y_0)]}{[(\alpha_n^2 - S_1 S_2) Y_0 - (S_1 + S_2)] \cos \alpha_n Y_0 + \alpha_n [(S_1 + S_2) Y_0 + 2] \sin \alpha_n Y_0} , \tag{47}$$

$$R_n(T) = \int_0^T I_0(T') e^{-\nu_n (T - T')} dT' . \tag{48}$$

It should be noted that the coefficients A_n and B_n listed above are independent of the form of the light excitation. They are defined exclusively in terms of semiconductor parameters. Thus, to determine the specimen photovoltaic response to different illuminations, only (48) need be calculated for each case of interest. For example, if the semiconductor is exposed to radiation of constant intensity I_0 that begins at $T=0$, we have $I_0(T)=I_0(T>0)$ and (48) gives[10]

$$R_n(T)=(I_0/\nu_n)(1-e^{-\nu_n T}) . \tag{49}$$

For an illumination at constant intensity I_0 that begins at $T=0$ and ends at $T=T_1$ we have

$$\begin{aligned} I_0(T)&=I_0 \quad (0<T<T_1)\\ &=0 \quad (T>T_1) . \end{aligned} \tag{50}$$

Substitution of the above into (48) gives

$$\begin{aligned} R_n(T)&=(I_0/\nu_n)(1-e^{-\nu_n T}) \qquad (0<T<T_1)\\ &=(I_0/\nu_n)(e^{-\nu_n(T-T_1)}-e^{-\nu_n T}) \quad (T>T_1) . \end{aligned} \tag{51}$$

For a sinusoidal light pulse of peak intensity I_0 and duration T_1, setting $\omega=\pi/T_1$, one has

$$\begin{aligned} I_0(T)&=I_0\sin\omega T \quad (0<T\leq T_1)\\ &=0 \qquad\qquad (T\geq T_1) . \end{aligned} \tag{52}$$

In this case (48) gives

$$\begin{aligned} R_n(T)&=\frac{I_0(\nu_n\sin\omega T-\omega\cos\omega T+\omega e^{-\nu_n T})}{\nu_n^2+\omega^2} \quad (0<T\leq T_1)\\ &=\frac{I_0\omega(e^{-\nu_n(T-T_1)}+e^{-\nu_n T})}{\nu_n^2+\omega^2} \qquad (T\geq T_1) . \end{aligned} \tag{53}$$

In this way solutions for a variety of light excitations are easily obtained.[11]

The photovoltaic theory may be extended to include extrinsic semiconductors also. However, solutions are readily obtained only for small illumination intensities. In such cases, the excess-carrier concentration δp is everywhere small compared to the equilibrium majority carrier concentration and D^* and σ^* reduce to D_0 and σ_0, where the zero subscripts indicate equilibrium values. Likewise, the excess-carrier lifetime τ becomes the minority carrier lifetime τ_0. With the above identification, (44) and (45) apply. For intermediate illumination intensities D^* is concentration dependent. Thus, the continuity equation is nonlinear and cannot readily be solved. Unlike the steady-state case, the above situation prevails in the large intensity regime also, particularly at the onset of illumination. Therefore, caution is to be exercised in applying the time-dependent theory to such cases.

The photovoltaic theory may be used to describe the transverse Dember effect that occurs in naturally anisotropic semiconductors. In this case the quantities $\overleftrightarrow{\sigma_n}$ and $\overleftrightarrow{\sigma}$ represent the electron and hole *conductivity* tensors that characterize the particular material under consideration. It is clear, however, that the theory applies only to cases for which the transport tensors are of the form indicated by (1) and (2). Thus, in experimental studies, properly oriented specimens must be employed. The form of the tensors considered herein is entirely one of convenience, such as to make the problem essentially one dimensional. The more general three-dimensional problem is quite formidable and remains unsolved.

The theory may also be used to describe photovoltaic effects in cubic semiconductors for which anisotropies have been externally created. In the photopiezoresistance effect, elastic strain produces the required anisotropies. In this case $\overleftrightarrow{\sigma_n}$ and $\overleftrightarrow{\sigma_p}$ are to be regarded as *piezoconductivity* tensors. It might be noted that these tensors are required to be symmetric so that the two anisotropy factors, a^* and a, are equal for this case.

In the photomagnetoelectric effect, an external magnetic field $\vec{H}$ produces the conductivity anisotropies. Thus, $\overleftrightarrow{\sigma_n}$ and $\overleftrightarrow{\sigma_p}$ represent *magnetoconductivity* tensors in this case. With $\vec{H}$ along the positive z axis as defined in Fig. 1, we have a standard Hall-effect geometry and the magnetoconductivity tensors have the form indicated by (1) and (2). These tensors are such that[12]

$$\begin{aligned} &\sigma_{nxx}=\sigma_{nyy} , \quad \sigma_{pxx}=\sigma_{pyy} ;\\ &\sigma_{nxy}=-\sigma_{nyx} , \quad \sigma_{pxy}=-\sigma_{pyx} . \end{aligned} \tag{54}$$

In addition, one may define[12]

$$\begin{aligned} \tan\theta_n&=\sigma_{nxy}/\sigma_{nyy} ,\\ \tan\theta_p&=\sigma_{pxy}/\sigma_{pyy} , \end{aligned} \tag{55}$$

where θ_n and θ_p are Hall angles for electrons and holes, respectively. Thus, one obtains

$$a=-a^*=\tan\theta_p-\tan\theta_n \tag{56}$$

for the anisotropy factors in this case. For small Hall angles and negligible magnetoresistance, the anisotropy factor $a=\theta$, where

$$\begin{aligned} \theta&=\theta_p-\theta_n ,\\ &=\theta_p+|\theta_n| , \end{aligned} \tag{57}$$

and (8)–(10) reduce to the van Roosbroeck equations[8] for the photomagnetoelectric effect. Thus, the theory given herein is a time-dependent theory for the photomagnetoelectric effect, one not limited by the small-Hall-angle approximation, and the effect itself is seen to be a special case of the photovoltaic effect that generally occurs in anisotropic semiconductors.

III. TRANSIENT PHOTOPIEZORESISTANCE EFFECT IN GERMANIUM

As a specific application of the theory, let us consider the photopiezoresistance effect in more detail. The photopiezoresistance effect was first observed in germanium by Kikoin and Lazarev.[4] Recently, a more complete set of observations was reported by Hahn and Schetzina.[6] In both cases, however, only steady-state properties were investigated. In this section, the results of a series of experiments undertaken to observe the *transient* photopiezoresistance effect in this semiconductor are discussed. The experimental results are then compared with those predicted by the ambipolar theory.

Two germanium specimens were prepared from an undoped single-crystal ingot for use in these experiments. The ingot was oriented using the optical-reflection technique and rectangular parallelopipeds, having dimensions $x_0 = 1.50$ cm, $y_0 = 0.10$ cm, $z_0 = 0.45$ cm, were cut from the ingot with a diamond-blade saw. The crystallographic orientation of these specimens is illustrated in Fig. 2. In the figure a $(1\bar{1}0)$ plane slab is shown with [111] and $[11\bar{2}]$ crystal directions indicated. The specimen axes are defined such that ϕ is the angle between the x axis and the [111] crystal direction. A specimen cut as shown and compressed along its x axis will display the required electrical anisotropy. A plot of the anisotropy factor for germanium versus orientation angle ϕ is also shown in the figure. The curve was obtained by first expressing the anisotropy factor in terms of appropriate piezoresistance coefficients[5] and then computing its value for various orientation angles. The parameter values used in these computations are listed in Table I. Both of the specimens used in the experiments were oriented such that $\phi = 29°$, in order to maximize the effect for a given compressional stress.

The two germanium samples were subjected to different surface treatments. The illuminated surfact (at $y = 0$) of each was lapped, polished, and etched with *CP4A* to obtain a low-surface-recombination velocity. The dark surface (at $y = y_0$) of specimen I was prepared in similar fashion, whereas, for specimen II, this surface was lapped with a 20-μm abrasive to obtain a high-surface-recombination velocity. In all other respects, the two specimens were identical.

The ends of the specimen to be compressed were cemented into slotted brass cylinders that were encased in nylon cups for electrical insulation. The brass cylinders also served as large-area electrical contacts. These contacts proved to be of low resistance but did produce small photovoltages with the specimen illuminated but unstressed. In all cases, however, zero-stress photovoltages were less than 1% of the signals observed with the specimen under appreciable compression and were, therefore, neglected. Compressional forces were applied to the specimen with a mechanical vise. Force levels were monitored with a calibrated load cell.

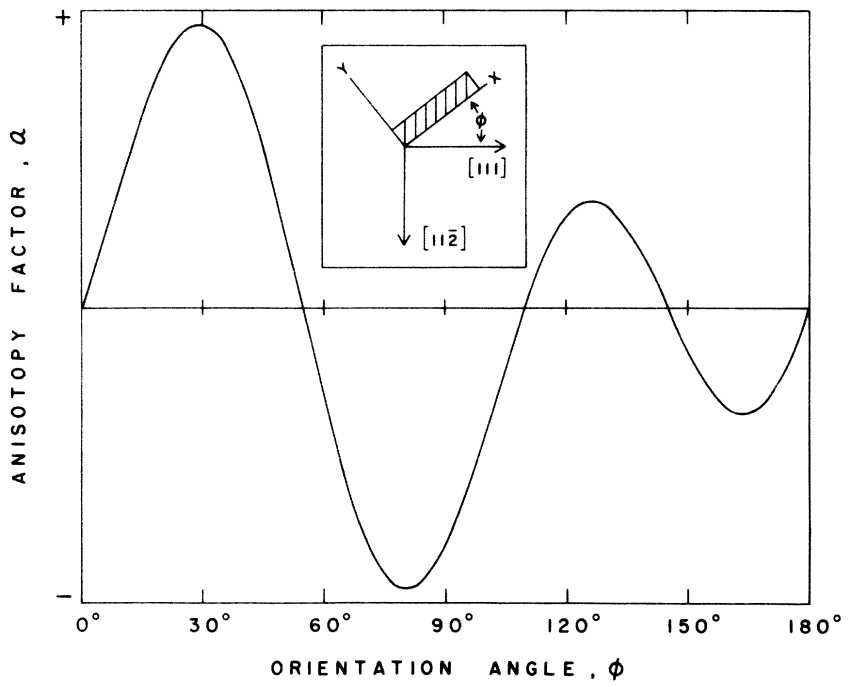

FIG. 2. Anisotropy factor a vs orientation angle ϕ for germanium. In the insert, the specimen x and y axes are shown.

TABLE I. Parameters used in calculations discussed in text.

Parameter	Value
Electron mobility[a]	3900 cm^2/V sec
Hole mobility[a]	1900 cm^2/V sec
Piezoresistance coefficients[b]:	
π_{n11}	-5.2 (10^{-12} cm^2/dyn)
π_{n12}	-5.5 (10^{-12} cm^2/dyn)
π_{n44}	-138.7 (10^{-12} cm^2/dyn)
π_{p11}	-10.6 (10^{-12} cm^2/dyn)
π_{p12}	-5.0 (10^{-12} cm^2/dyn)
π_{p44}	98.6 (10^{-12} cm^2/dyn)
Surface-recombination velocities:	
s_1	100 cm/sec
s_2 (specimen I)	100 cm/sec
s_2 (specimen II)	10 000 cm/sec
Excess-carrier lifetime[c]	500 μsec
Temperature	298 °K
Quantum efficiency	1.0 electron-hole pairs per photon
Equilibrium carrier concentration[d]	2×10^{13} cm^{-3}

[a]Reference 16.
[b]Reference 17.
[c]Determined via transient photoconductivity experiment.
[d]Representative values.

In the initial experiments, the germanium samples were illuminated with chopped white light from a calibrated 1000-W tungsten-halogen lamp. The mechanical chopping system produced trapezoidal light pulses of 3.5 msec duration having 50-μsec rise and fall times. In these experiments, the lamp was positioned such as to produce an illumination intensity $I_0 = 10^{17}$ photons/cm^2 sec (±5%) at the surface of the specimen. All illumination intensities quoted in this paper are those giving rise to fundamental absorption only and have been corrected for reflection losses.

In the second set of experiments a General Radio type 1531-AB xenon stroboscope was used as a light source. The particular unit employed, when operated at 60 Hz, produced relatively intense light pulses of 2-μsec duration. The strobe was placed such that the peak light intensity at the illuminated semiconductor surface was 10^{19} photons/cm^2 sec (±20%).

All of the experiments were performed at room temperature with the specimens in air. Photovoltages were measured with a Tektronix type 555 oscilloscope using type 1A2 plug-in units. The experiments were performed as a function of increasing stress with photographs of the oscilloscope trace taken at each stress level. The specimens were subjected to maximum stresses of 5×10^9 dyn/cm^2.

In all of the experiments the observed photovoltages were found to increase linearly with stress. Typical plots of the photovoltage versus time exhibited by specimens I and II, when illuminated with chopped white light, are shown in Fig. 3. The curves shown in this figure were recorded with the specimens under a compressive stress of 5×10^9 dyn/cm^2. The photovoltage curve for specimen I (etched dark surface) shows a relatively sharp peak at $t \approx 50$ μsec followed by relaxation to a steady-state value of about 25 mV. For specimen II (abraded dark surface), the initial peak is absent. However, the steady-state photovoltage exhibited by this specimen is approximately three times greater than that shown for specimen I. The differences in the two curves are clearly attributable to different dark-surface treatments. The above behavior is reminiscent of that reported by Bulliard,[13] Hall,[14] and Gridin and Elesin[15] in their investigations of the transient photomagnetoelectric effect in germanium. In view of the foregoing discussion, such similarities are to be expected.

In Fig. 4 the photovoltaic response of specimen I, when illuminated with 2-μsec light pulses from the xenon strobe, is shown for several stress levels. The curves illustrate both the large magnitude of the photopiezoresistance effect for this type of illumination as well as its linear dependence on stress. Photovoltage curves, nearly identical in both shape and magnitude, were also recorded for specimen II. Thus, for relatively fast rise-time light pulses, the recombination velocity at the dark

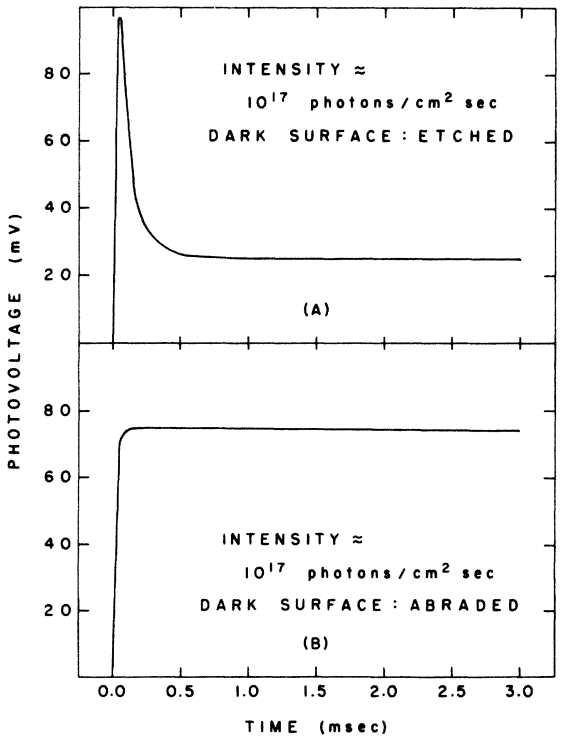

FIG. 3. Photovoltages displayed by (A) specimen I, and (B) specimen II when exposed to chopped white light from tungsten lamp.

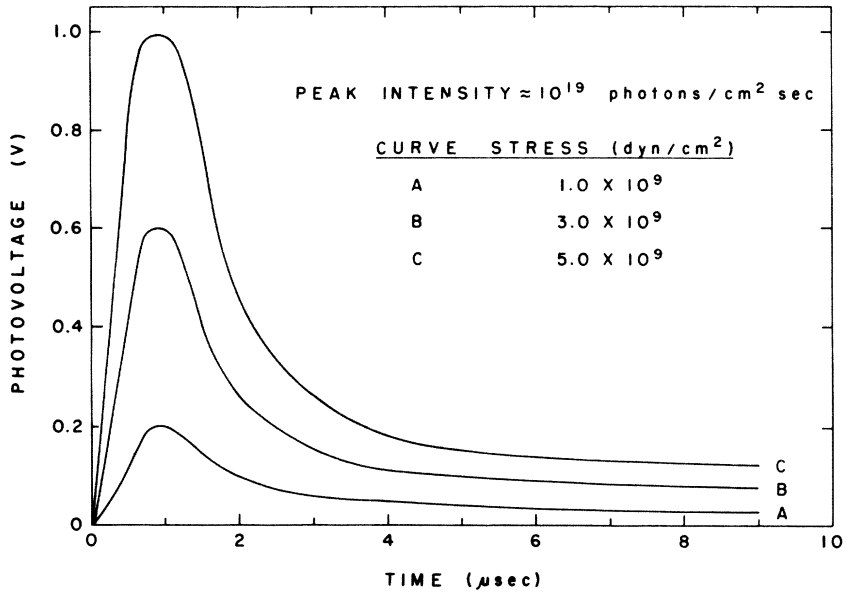

FIG. 4. Photovoltages displayed by specimen I when illuminated with 2.0-μsec light pulses from xenon strobe.

surface does not significantly affect the specimen response. This is expected since the photovoltage developed is determined by the evolution of the photogenerated carrier distribution with time. At the onset of illumination, the number density of excess carriers of the illuminated surface is large, while that throughout most of the bulk and at the dark surface is zero. The diffusion of excess carriers into the interior of the specimen is, thus, initially determined by bulk properties rather than dark-surface properties. Only for (dimensionless) times $T > Y_0$ do appreciable numbers of electrons and holes reach the vicinity of the dark surface, at which point the recombination velocity at this surface affects the spatial distribution of carriers and, therefore, the magnitude of the photovoltage. It is for this reason that steady-state values are quite sensitive to dark-surface preparations, as evidenced by the curves shown in Fig. 3, whereas the initial transient is not.

Let us now turn our attention to a quantitative description of the curves shown in Figs. 3 and 4. Theoretical expressions for the open-circuit photovoltage per unit length for the above types of light excitations may be obtained from (45) and (48). The relaxation to equilibrium that occurs at the termination of the chopped tungsten light pulse will not be considered, in which case the illumination intensity may be expressed as

$$I_0(T) = (T/T_1)I_0 \quad (0 < T \leq T_1)$$
$$= I_0 \quad (T \geq T_1) \tag{58}$$

with $I_0 = 10^{17}$ photons/cm^{2}sec and $T_1 = t_1/\tau$, where $t_1 = 50$ μsec is the rise time of the light pulse. Using (48) one then obtains

$$R_n(T) = I_0\left(\frac{e^{-\nu_n T} + \nu_n T - 1}{\nu_n^2 T_1}\right) \quad (0 < T \leq T_1)$$
$$= I_0\left(\frac{e^{-\nu_n T} - e^{-\nu_n (T-T_1)} + \nu_n T_1}{\nu_n^2 T_1}\right) \quad (T \geq T_1)\,. \tag{59}$$

The light pulse from the strobe can be represented by a sinusoidal function of the form given by (52), in which $I_0 = 10^{19}$ photons/cm^{2}sec and $\omega = \pi\tau/t_1$, where $t_1 = 2$ μsec. Apart from a small relaxation tail, the above is a good approximation to the pulse shape determined experimentally using a fast silicon photodiode. The time-dependent function $R_n(T)$ is then given by (53) for this type of illumination.

In order to generate theoretical photovoltage curves, all of the stress-dependent quantities that appear in the theory were evaluated using methods discussed in Ref. 5. Parameter values used in these calculations are listed in Table I. A computer was then employed to obtain roots of the transcendental equation (42) and to evaluate (45) at selected times. To ensure proper convergence, 500 terms were included in (45) for the excitation given by (58). In the time range $t < 2$ μsec, 6000 terms were included in the series solution for the excitation given by (52). The results of these calculations are illustrated by the curves shown in Figs. 5 and 6, in which the *total photovoltage* for a specimen of length 1.50 cm is plotted. The photovoltage curve obtained for specimen I for the chopped tungsten-lamp illumination is shown in Fig. 5A. It is seen that the theory correctly predicts the initial peak in the photovoltage that is observed

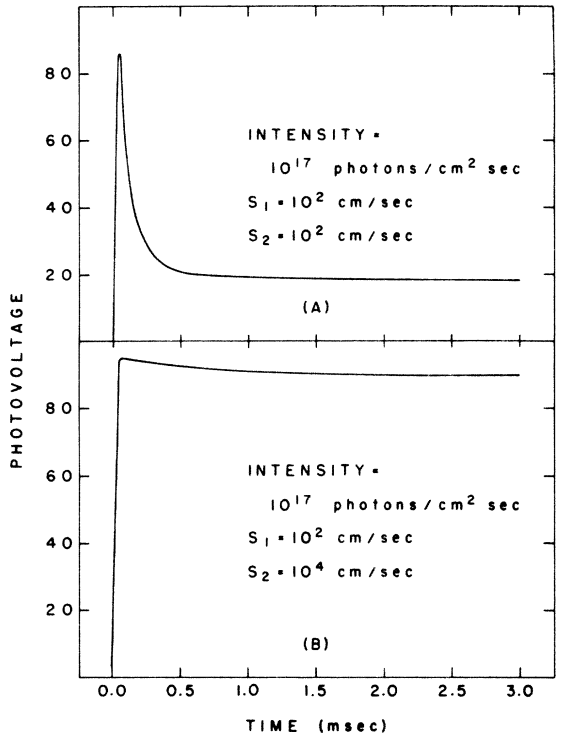

FIG. 5. Theoretical photovoltage curves obtained for (A) specimen I and (B) specimen II for chopped-white-light illumination.

experimentally. In addition, relatively good quantitative agreement between theory and experiment is indicated. In Fig. 5(b), the theoretical photovoltage curve obtained for specimen II is shown. The large photovoltage peak is absent in this case, although a slight relaxation is indicated.

At any given time, the specimen photovoltage is directly proportional to the difference in carrier concentrations at the illuminated and dark surfaces, respectively, and inversely proportional to the conductance, as is indicated by (26). The peak in the photovoltage curve shown in Fig. 5(a) is due to the rapid generation of excess carriers at the illuminated surface during which time the increase in conductance, proceeding via diffusion, is negligible. Thus, the numerator in (26) is initially large and the denominator is small. At later times, both the concentration of carriers at the dark surface and the photoconductance are appreciable and the photovoltage decreases. The absence of an initial peak in the curve shown in Fig. 5(b) is due to the large dark-surface-recombination velocity associated with specimen II which, in effect, locks the number density of carriers at this surface to the equilibrium value for all times. Thus, the numerator in (26) is always large and the large steady-state photovoltage which results masks the initial transient. For illumination intensities $I_0 > 10^{17}$ photons/cm^{2}sec, however, the theory predicts an initial photovoltage peak for this specimen also. In subsequent experiments, in which an intensity $I_0 = 5 \times 10^{17}$ photons/cm^{2}sec was used, such behavior was observed.

The above physical description clarifies why large transient photovoltages develop in the limit of intense fast-rise-time light excitations. In Fig. 6, theoretical photovoltage curves for the sinusoidal excitation given by (52) are displayed. The curves shown in this figure are in general agreement with the experimental curves shown in Fig. 4. The theory gives peak photovoltages to within 10% of those actually observed and correctly pre-

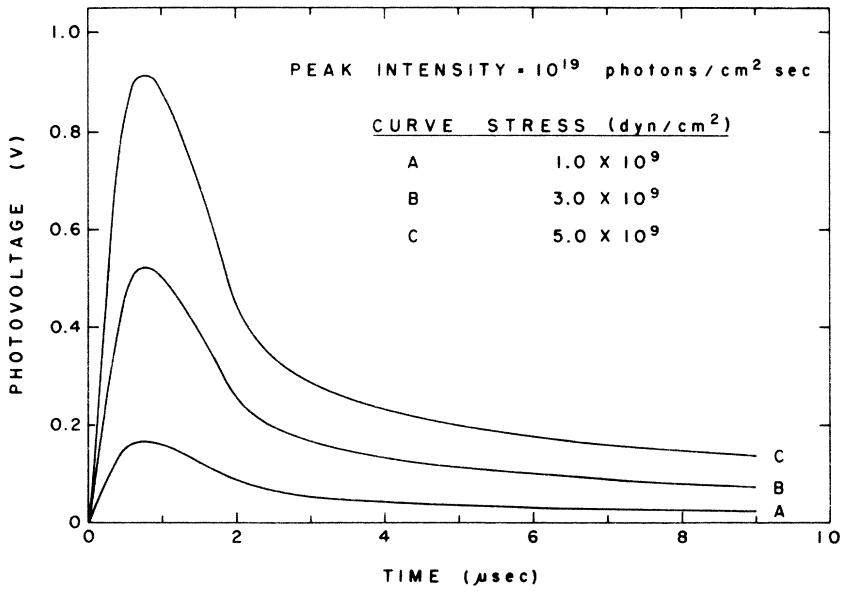

FIG. 6. Theoretical photovoltage curves obtained for specimen I for xenon-strobe illumination.

dicts the linear stress dependence. In addition, the theoretical curves are found to be independent of the value of the dark-surface-recombination velocity used in the calculation.

The experimental results discussed above illustrate the close similarity of the transient photomagnetolectric and photopiezoresistance effects. The results also indicate that the transient photopiezoresistance effect is often much larger than the steady-state effect. In addition, the general agreement between theory and experiment lends support to the validity of describing processes of this type via an ambipolar approach.

ACKNOWLEDGMENT

The authors are pleased to acknowledge illuminating discussions with Professor F. Lado concerning the use of the Laplace transformation.

---

*Work supported in part by the Office of Naval Research and by the Research Corporation.

[1]I. P. Zhad'ko, E. I. Rashba, V. A. Romanov, I. M. Stakhira, and K. D. Tovstynk, Fiz. Tverd. Tela 7, 1777 (1965) [Sov. Phys.—Solid State 7, 1432 (1965)].

[2]D. Genzow, Phys. Status Solidi A 7, K77 (1971); Phys. Status Solidi B 55, 547 (1973).

[3]W. van Roosbroeck and W. B. Pfann, J. Appl. Phys. 33, 2304 (1962).

[4]I. K. Kikoin and S. D. Lazarev, Zh. Eksp. Teor. Fiz. 47, 780 (1964) [Sov. Phys.—JETP 20, 521 (1965)].

[5]R. M. Shah and J. F. Schetzina, Phys. Rev. B 5, 4014 (1972).

[6]T. S. Hahn and J. F. Schetzina, Phys. Rev. B 7, 729 (1973).

[7]I. K. Kikoin and M. M. Noskov, Physik Z. Sowjetunion 5, 586 (1934).

[8]W. van Roosbroeck, Phys. Rev. 101, 1713 (1956).

[9]These tensors are more general in form than those used in Ref. 5.

[10]One obtains solutions for the steady state as $T \to \infty$ in (49). However, closed-form solutions to (25) and (26) may be obtained directly from Eqs. (27)–(29) for the constant-illumination case. Such solutions are found in the literature and will not be discussed here.

[11]In choosing the dimensionless time scale $T = t/\tau$, we have made the tacit assumption that τ is a constant, independent of δp. This is generally true only in the small modulation regime. For large illumination intensities, which lead to appreciable excess-carrier densities, the lifetime becomes concentration dependent. Even in such cases, however, the transient solutions given herein are not significantly affected for times $t \ll \tau$. In this time range, the distribution of excess carriers within the semiconductor is primarily determined by diffusive rather than recombination processes. The reader should realize, however, that long-time or steady-state solutions for large illuminations are only approximately correct under the constant lifetime assumption. In fact, the discrepancy between theory and experiment mentioned in Ref. 6 may be partially due to a concentration-dependent lifetime.

[12]A. C. Beer, in *Solid State Physics*, edited by F. Seitz and D. Turnbull (Açademic, New York, 1963), Vol. 4.

[13]H. Bulliard, Phys. Rev. 94, 1564 (1954).

[14]L. H. Hall, Phys. Rev. 97, 1471 (1955).

[15]V. A. Gridin and V. F. Elesin, Fiz. Tverd. Tela 7, 730 (1965) [Sov. Phys.—Solid State 7, 585 (1965)].

[16]M. B. Prince, Phys. Rev. 91, 282 (1953).

[17]C. S. Smith, Phys. Rev. 94, 42 (1954).